Comparison of Aerodynamic Characteristics of Morphing and Conventional Wings

Mir Hossein NEGAHBAN[1], Ruxandra Mihaela BOTEZ*,[1]

*Corresponding author
[1]LARCASE - Laboratory of Applied Research in Active Controls,
Avionics and Aeroservoelasticity,
École de Technologie Superieure (ÉTS), University of Quebec,
Montreal, QC, Canada
ruxandra.botez@etsmtl.ca*

DOI: 10.13111/2066-8201.2025.17.2.5

Received: 18 March 2025/ Accepted: 12 May 2025/ Published: June 2025

Abstract: *The present research investigates the advantages of a morphing versus a hinged flap. The morphing wing model is equipped with a morphing trailing edge, while the conventional wing has a hinged flap system. The aerodynamic and fight dynamics characteristics of both wings are evaluated, and a comparison is drawn to find out how the morphing wing enhances the flight performance in cruise flight conditions in terms of flight range increase. For this purpose, gradient-based aerodynamic optimization is performed to find the ideal configuration of a morphing flap in a cruise flight with the objective of increasing flight range. Finally, the aerodynamic characteristics of optimized morphing and hinged wings are compared, including aerodynamic loads, efficiency, turbulence, and flight range. The findings showed that the morphing wing extended the flight range by 18% in comparison to the hinged wing configuration.*

Key Words: *Morphing wing, Flight range, aerodynamic optimization*

1. INTRODUCTION

The sheer volume of flights results in significant CO2 emissions. The impact of aviation on carbon output became particularly evident during the pandemic, when data captured a substantial decline in emissions before and during the global lockdown. The drastic reduction in flights led to a considerable decrease in aviation-related carbon emissions compared to other types of transportation, such as ground transportation and industrial activities [1]. Given its undeniable impact on climate change, minimizing carbon emissions has become a critical priority for the aeronautics industry.

In pursuit of sustainable aviation, various industrial and academic projects have been dedicated to reducing CO2 emissions. Among these efforts, flight trajectory optimization has been explored, with Airbus' UpNext project [2] introducing the "Fello'fly" concept, which has demonstrated at least a 5% reduction in carbon emissions per flight. However, most of research in Green Aviation focuses on aircraft design improvements, encompassing aerodynamic, propulsive, and structural innovations. Aerodynamic enhancements, such as drag reduction strategies, have played a significant role in lowering fuel consumption and improving its efficiency.

Morphing wing technology has emerged as a promising approach for next-generation eco-friendly aircraft by enabling reduced drag, lower fuel consumption, and decreased structural weight. Various morphing wing concepts have been investigated over the past decades, and among these investigations, trailing edge morphing has attracted particular interest.

The structural and aerostructural analyses of trailing edge morphing have gained momentum, supported by numerous research efforts. Several morphing conceptual designs have been introduced in the past decades, such as upper surface [3-6], winglet [7], span [8], camber [9-12], sweep [13], chord [14], leading edge [15-17], and twist [18] morphing. Although conceptual design exists for various morphing configurations, including leading edge and upper surface morphing, only a few of them have been successfully flight-tested.

One of the pioneering projects, the Mission Adaptive Wing Project [19], successfully integrated active camber morphing into a fighter jet. However, due to the complexity and weight of the actuation system, the project was discontinued. Ting et al. [20, 21] studied structural and aerodynamic optimizations, revealing lift-to-drag ratio gains of 2-16% and drag reductions of up to 8.4% under varying flight phases.

Urnes et al. [22] examined the variable camber trailing edge system's potential for future aircraft, demonstrating improvements in lift, drag reduction, weight reduction, and maneuverability.

Their findings suggested that this technology could enhance both lift for takeoff and landing and cruise efficiency through optimized wing twist control. Woods et al. [23] investigated morphing flap transition parts to address spanwise edge gaps, successfully eliminating vortex formation and improving aerodynamic efficiency.

Similarly, Ninian and Dakka [24] compared morphing flaps with their conventional designs, showing a 10.8% lift increase and a 13.6% improvement in the lift-to-drag ratio. Their experimental acoustic analysis also demonstrated a 50% reduction in noise levels with morphing wings compared to their traditional configurations. Lyu et al. [25] employed gradient-based optimization techniques to refine trailing edge designs, achieving drag reductions in off-design and on-design conditions, leading to an estimated 1% reduction in cruise fuel consumption.

Meanwhile, Communier et al. [26] introduced a novel morphing trailing edge design incorporating small vertical incisions, which yielded lower drag and higher aerodynamic efficiency than conventional flaps.

To further enhance aerodynamic performance, Khorami et al. [27] patented an elastic morphing structure to eliminate discontinuities in the trailing edge flap's side edges, reducing aeroacoustic noise without compromising efficiency. Rivero et al. [28] experimentally evaluated the FishBack morphing concept and found that it significantly improved lift-to-drag ratios, with gains ranging from 50% to 200% over baseline airfoil configurations.

Based on these advancements, the present study aims to optimize a morphing wing for cruise flight conditions to increase its flight range. So far, no high-fidelity optimization has yet been performed on a morphing trailing edge to enhance its flight performance. This research utilizes an unmanned aerial system UAS-S45, to optimize a Morphing Trailing Edge (MTE) for cruise flight with the aim of increasing overall flight range.

A high-fidelity optimization approach using gradient-based algorithm and the discrete adjoint method is applied to determine the optimal morphing wing configuration for cruise flight. The main objective is to optimize the fight range and compare the results with hinged flap configuration to discover the superiority of morphing wings. This research aims to further advance the practical implementation of morphing trailing edge technology in future aircraft design.

2. METHODOLOGY

Removing the discontinuities on the wing offers significant benefits by minimizing turbulence at the gaps, thereby improving the flow laminarity, reducing drag, and ultimately enhancing lift. As the primary control surfaces of a wing, eliminating the gaps and achieving smooth flap deformation will undoubtedly enhance aerodynamic efficiency.

This study examines the morphing wing in the cruise flight condition, with the objective of improving flight range. Figure 1 presents the morphing wing featuring a Morphing Trailing Edge (MTE).

As shown in Fig. 1, the flap extends over 30% chordwise and 43% spanwise, including its transition sections.

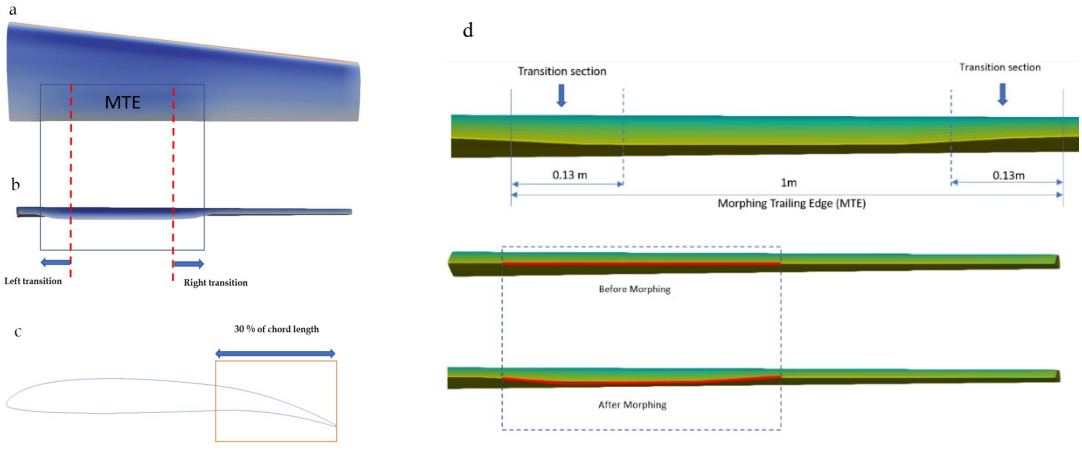

Fig. 1 – Schematics of a Morphing Trailing Edge (MTE). a) top view, b) rear view after morphing, c) side view, d) MTE before and after morphing with its actual dimensions

2.1 Optimization with DAFoam

A high-fidelity optimization algorithm, which utilizes an object-oriented discrete adjoint method, where the flow solver OpenFOAM is integrated directly into the optimization iterations. This methodology provides significantly more accurate results compared to lower-fidelity solvers, which are commonly used in the literature.

This framework was introduced by Towara et. al [29], utilizing Automatic Differentiation (AD) for derivative calculations.

However, due to the substantial computational cost of AD, particularly for shape optimization, it is not well-suited for solving complex aerodynamic problems.

To overcome this limitation, the Multidisciplinary Design Optimization (MDO) laboratory at the University of Michigan developed a new optimization framework [30], by which the efficiency of the discrete adjoint (DA) method was improved by replacing AD with an accelerated Finite Difference (FD) technique, making adjoint-based optimization with OpenFOAM to be the best choice for problems with hundreds of design variables. Moreover, this algorithm establishes a seamless interaction between OpenFOAM and Python libraries. The OpenFOAM layer comprises the flow solver and the graph coloring solver, while the Python layer handles mesh deformation and optimization setup.

Figure 2 shows the complete optimization workflow, with distinct colors representing the OpenFOAM and Python layers.

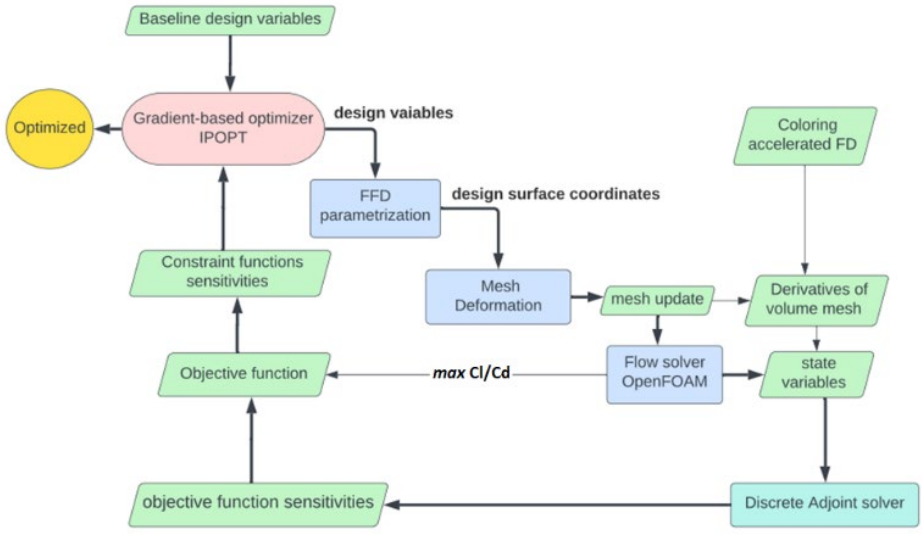

Fig. 2 – DAFoam Optimization framework

2.2 Free-Form Deformation (FFD)

Before beginning the optimization process, the wing model must first be generated, and the parametrization technique choice plays a crucial role in determining the final optimization outcomes. An effective parametrization method should be capable of covering a broad design space while maintaining the integrity of design variables.

One widely used approach is the Free-Form Deformation (FFD), which belongs to the category of deformative parametrization techniques. Initially introduced by Sederberg and Parry in 1986 [31], the FFD method has undergone multiple refinements over the years, leading to its application in real-world engineering challenges [32-34]. In its earliest form, the FFD method relied on tri-variate Bernstein polynomials to define control points within the deformation block [35].

However, later advancements incorporated alternative polynomial formulations, such as tri-variate Bezier and Non-Uniform Rational B-Splines (NURBS). The fundamental principle of FFD involves enclosing the target object (such as an aircraft or its wing) within a deformable block, where any modifications made to the block control points induce shape changes in the embedded geometry.

For complex three-dimensional optimization tasks, such as full-wing or aircraft shape refinement, the number of design variables can easily reach the order of hundreds. The FFD operates by modifying geometric variations rather than by directly manipulating the geometry [36].

This feature significantly reduces the sensitivity to the number of design variables, making it particularly well-suited for optimization problems that require handling extensive shape modifications.

Mathematically, if we define $\bar{g}$ as the baseline geometry and $\Delta\bar{G}$ as the corresponding shape variation, the total modified shape can be expressed as:

$$\bar{\mathbf{G}}_{defomed} = \bar{\mathbf{g}} + \Delta\bar{\mathbf{G}} \tag{1}$$

The geometrical change $\Delta\bar{G}$ during the aerodynamic optimization encompasses all kinds of variations, as shown in Eq. (2):

$$\Delta\overline{\mathbf{G}} = \delta\overline{\mathbf{G}}_{twist} + \delta\overline{\mathbf{G}}_{camber} + \delta\overline{\mathbf{G}}_{thickness} + \delta\overline{\mathbf{G}}_{shear} + \delta\overline{\mathbf{G}}_{planform} \quad (2)$$

By specifying the degree of freedom of FFD control points, these variations are managed according to the morphing technique. The camber is the only necessary variation in the Morphing Trailing Edge (MTE). For example, in the MTE, only camber morphing is considered ($\delta\bar{G}_{camber} > 0$).

As this research focuses on the MTE, the wing's deformation is restricted to both downward and upward deformations.

The parametrization utilizes Free-Form Deformation (FFD) with two distinct FFD blocks governing the wing geometry.

The first block corresponds to the morphing flap section (red), while the second block (blue) represents the solid wing section, as shown in Figure 3.

For precise shape control, the FFD framework incorporates 30 control points along the span and 6 control points along the chord, resulting in 360 control points in total. However, only the trailing edge control points (colored green) are allowed to move, enabling flap deflection.

The remaining control points remain fixed with zero displacements. As a result, only 52 of the 360 control points actively participate in the morphing process, ensuring that the deformation remains confined to the flap while preserving the aerodynamic integrity of the main wing structure.

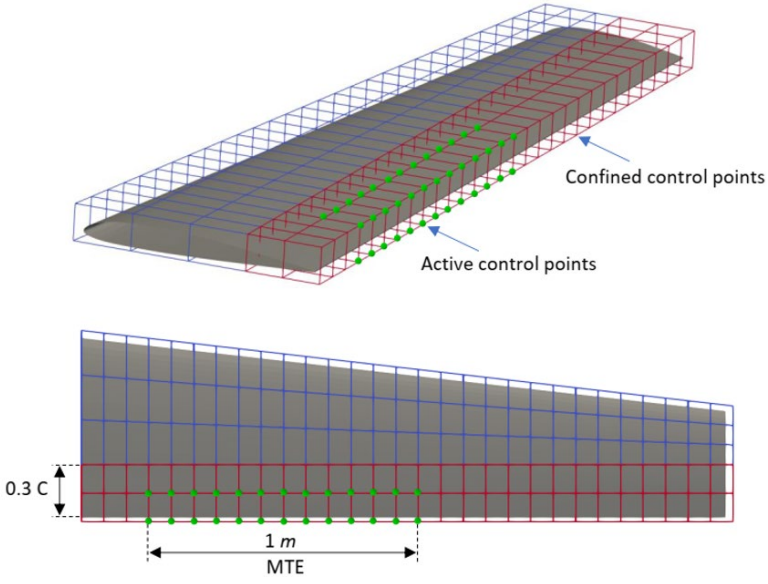

Fig. 3 – FFD block for the parametrization of the morphing trailing edge

2.3 Optimization framework

The purpose of this research is to find the optimized MTE for the cruise flight condition that is characterized by the specific goal of increasing flight range, as shown in Table 1, and Table 2 shows the details of the cruise flight.

Table 1 – The objective function of the MTE optimization

Flight condition	Objective	Obj. function
Cruise	Maximizing flight range	max (C_L/C_D)

Table 2 – Cruise flight condition characteristics for the UAS-S45

Flight condition	Speed (knots)	Reynolds number × 10^6	Altitude (ft)
Cruise	55	0.7	15,000

Table 3 shows the optimization setup, constraints, and objective function. The linear constraint is used to obtain an equal deformation in the spanwise direction. The upward and downward deflections are confined to 150 mm.

Table 3 – Optimization setup for maximizing range

Variables and Constraints	Explanation	number
$max\ C_L/C_D$	Objective function	4
w.r.t: Y	FFD control points	360
Subject to:		
$C_l \geq C_{l\,min}$	Constant function	1
$AOA_{initial}=AOA_{final}$	Constant angle of attack	1
$V \geq V_{initial}$	Volume constraint	1
$-150mm \leq \Delta y \leq 150\ mm$	Deflection limits	52
$\Delta y_{z=3}^{upper} = \Delta y_{z=15}^{upper}$	Linear constraint	52

2.4 Solver setup

The analysis is conducted for cruise flight conditions within the subsonic regime. The RANS equations are solved using the steady-state solver. For turbulence modeling, the Spalart-Allmaras is utilized due to its efficiency in handling aerodynamic simulations.

Regarding boundary conditions, the surface to which the wing is attached is set as a "symmetry" boundary, while all other boundaries are assigned the "inletOutlet" condition.

This setup allows the boundary to switch dynamically between "fixed value" when fluid enters the domain and "zero gradient" when fluid exits, ensuring a realistic representation of the aerodynamic environment.

3. RESULTS AND DISCUSSIONS

3.1 Range optimization

For aircraft powered by propeller engines, the total flight range R can be determined using the following equation [37]:

$$R = -\frac{\eta_p}{\gamma_p}\frac{C_L}{C_d}\ln\left(\frac{W_1}{W_2}\right) \tag{3}$$

In this equation, η_p represents the propulsive efficiency, while γ_p denotes the fuel consumption per unit weight. The terms W_1 and W_2 correspond to the aircraft's primary and final weight, respectively.

From Eq. (3), it is evident that the primary aerodynamic factor influencing the range is C_L/C_d. Consequently, improving lift to drag ratio directly enhances the aircraft's range.

To assess the benefits of a MTE design compared to a traditional hinged flap system, a comprehensive evaluation is conducted. This analysis involves comparing key aerodynamic parameters such as lift, drag, and the lift-to-drag ratio between the MTE, a conventional hinged wing, and a clean wing configuration. The goal is to determine the extent, to which the MTE technology enhances aerodynamic performance over conventional control surface designs. The aerodynamic characteristics of the three configurations MTE, clean wing, and hinged flap are illustrated in Figure 4, providing a comparative visualization of their performance metrics.

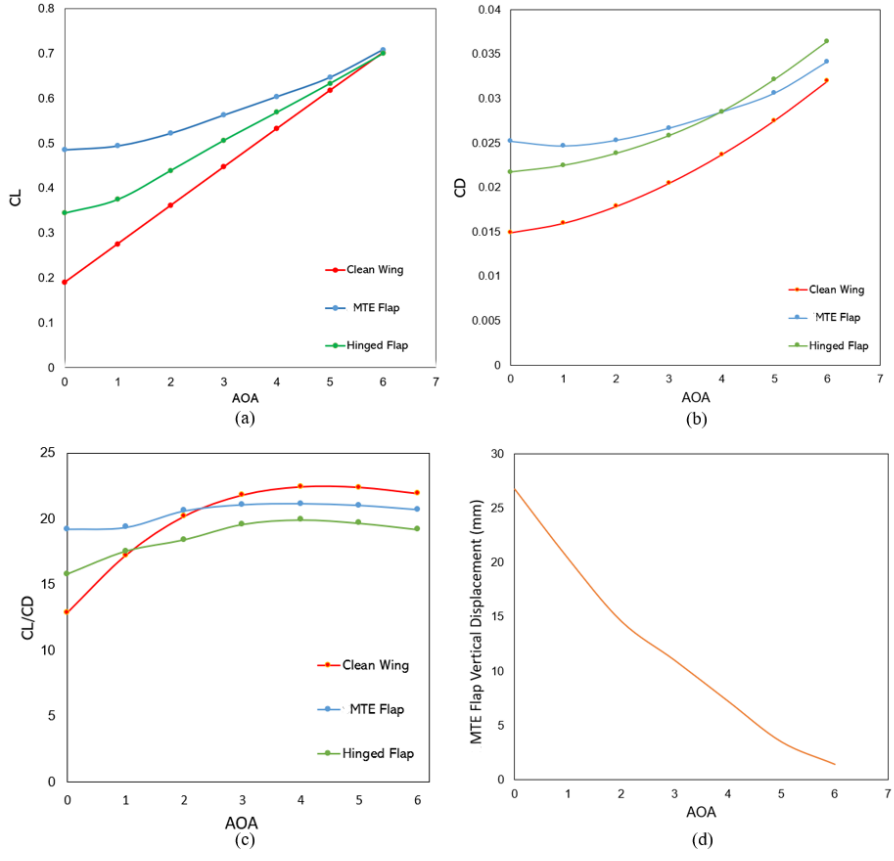

Fig. 4 – Aerodynamic performance comparison among the morphing wing, hinged wing, and clean wing configurations; a) lift coefficient, b) drag coefficient, c) C_L/C_d, d) flap deflection magnitude

As shown in Fig. 4-(c), beyond an angle of attack of 2.4°, the performance of the MTE deteriorates compared to the baseline wing. The best performance of hinged flap is limited to angles of attack up to 1°.

This suggests that MTE flap can operate efficiently over a broader range of angles (from 0° to 2.4) in contrast to the hinged flap, where the improvement over the clean wing is confined to angles of attack between 0° and 1°. Figure 5 compares the performance of the morphed MTE and deflected hinged flap.

The improvement in lift-to-drag ratio is primarily driven by the increased lift generation of the morphing wing, as seen in the lift coefficient graph Fig. 4-(a).

Despite the fact the drag of the MTE is higher than the hinged flap at certain AOAs, as shown in Fig. 4-(b), the additional generated lift compensates for this drag penalty, leading to a significant overall increase in aerodynamic efficiency. Specifically, the morphing wing achieves a 32% improvement over the clean wing and an 18% improvement over the hinged flap (Fig. 4-c).

Furthermore, as the angle of attack increases, the morphing flap deformation reaches zero as shown in Fig. 4-(d).

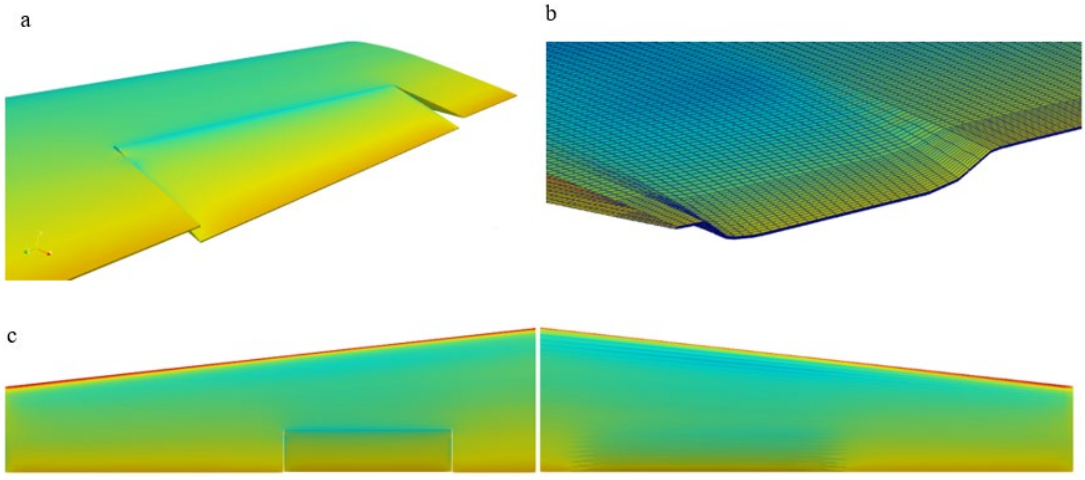

Fig. 5 – Comparison of a) hinged and b) morphing wings in the cruise flight

Figures 5-a and 5-b show the geometrical differences between an MTE and hinged flaps. Unlike the hinged flap, the MTE flap features sealed gaps between the flap and the main wing body, resulting in a smooth deformation.

As shown in Fig. 5-c, eliminating the gaps between the flap and the wing main body on the morphing wing has extended the flow laminarity, which reduces the likelihood of premature flow separation.

Additionally, Figure 6 (a)-(c) presents the entire UAS-S45 wing with both morphing and hinged configurations to provide a comprehensive comparison of pressure coefficient variations.

Furthermore, Figure 7 displays the pressure contours on the upper and lower surfaces of both the morphing and hinged wings from both top view and bottom view.

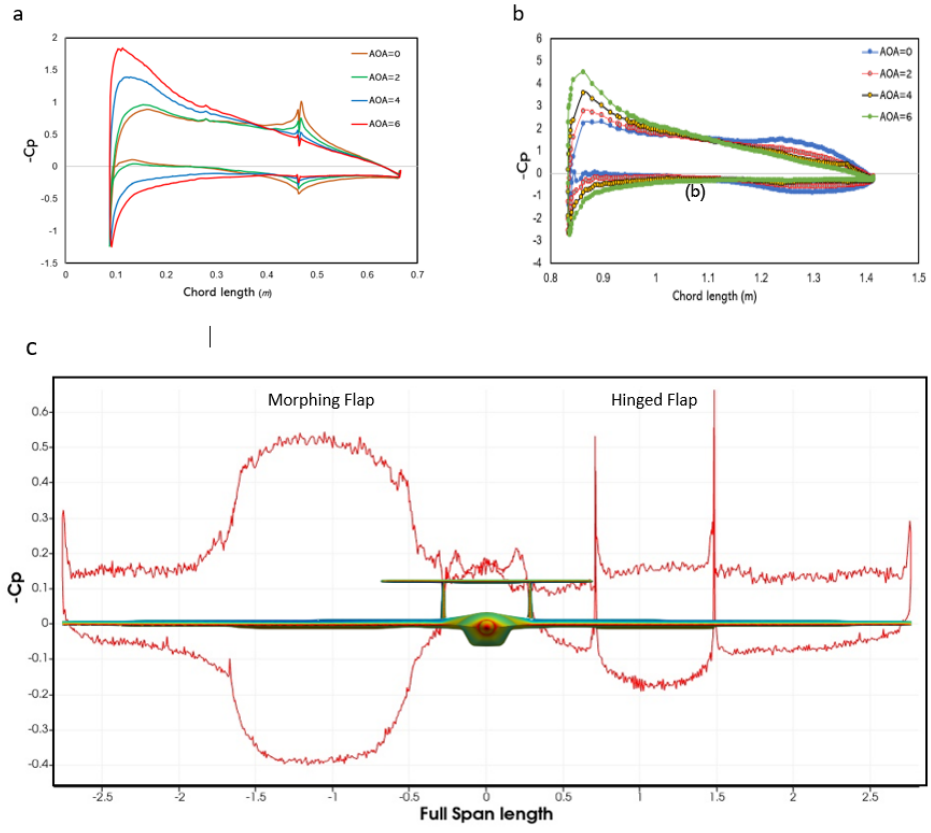

Fig. 6 – Pressure coefficient variations for MTE and a hinged flaps a) chordwise hinged wing, b) chordwise-MTE, c) spanwise

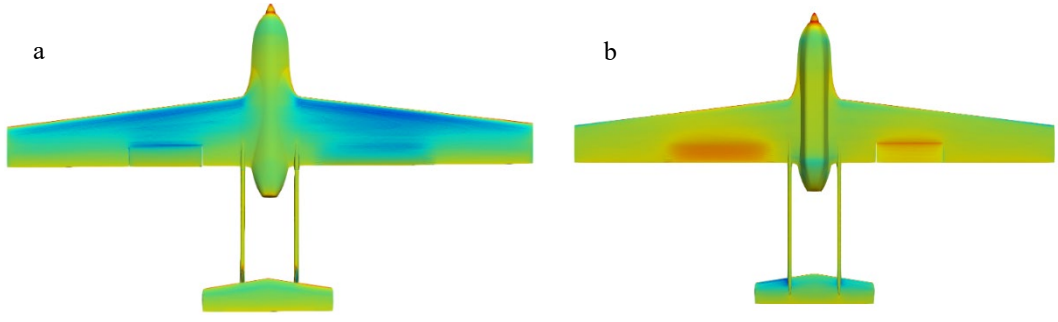

Fig. 7 – UAS-S45 Pressure contours equipped with hinged and MTE flaps, from a) top view, and b) bottom view

The pressure coefficient variations along wing chord and span in Figures 6 (a, b, c) depicts pressure variations around morphing and conventional flaps. In contrast, the morphing wing shown in Fig. 6-(c), eliminates these peaks, resulting in much smoother pressure variations. These pressure peaks are primarily caused by flow spilling from the high-pressure side to the low-pressure side due to the gaps.

Additionally, both the spanwise and chordwise pressure distributions (Fig. 6-a to 6-c)) depict that the morphing wing maintains a greater pressure differential compared to the hinged flap, leading to a higher lift.

Pressure coefficient increase is attributed to the flaps seamlessness, where the flap deformation contributes to a larger lifting surface.

While for the hinged flap, the region is truncated at the gap's start (Fig. 7-a), the morphing wing delays the transition from laminar to turbulent flow over the wings' upper surface by eliminating the gaps. The morphing wing preserves laminar flow all the way to the trailing edge tip (Fig. 7-a).

On the lower surface, the pressure contours in Figure 7-(b) further highlight the differences between the morphing and hinged flaps.

For the morphing wing, the highest pressure is created at the entire flap bottom surface-thanks to the removal of the gaps.

4. CONCLUSIONS

This study focused on cruise flight conditions with the objective of increasing flight range by replacing hinged flaps with morphing flaps to identify the optimal wing configuration. A comparison between the morphing wing and the hinged wing configuration highlighted several advantages of the morphing wing. These advantages included the extension of laminar flow over the upper surface, enhanced flow stability by reducing turbulence, and improved aerodynamic performance due to the sealing of gaps in the transition sections. This seamless characteristic resulted in an increase in the lift-to-drag ratio, and consequently, an improvement in flight range by 18% were obtained, in comparison to the hinged wing configuration, and by 32% in comparison to the clean wing. The maximum ranges' optimal angles of attack were also found, which ranged from 0° to 2.5°. This research demonstrated the benefits of morphing wings versus traditional hinged flaps and identified the optimal morphing wing configuration to enhance the flight range of the UAS-S45, leading to higher flight performance.

REFERENCES

[1] C. Le Quéré, R. B. Jackson, M. W. Jones, A. J. Smith, S. Abernethy, R. M. Andrew, A. J. De-Gol, D. R. Willis, Y. Shan, J. G. Canadell, Temporary reduction in daily global CO2 emissions during the COVID-19 forced confinement, *Nature climate change*, **10**(7), 647-653, 2020.

[2] * * * Airbus. *Exploring the possibilities of wake energy retrieval*, 2025 Available from: https://www.airbus.com/en/innovation/future-aircraft-operations/air-traffic-management/fellofly, (accessed 12 Febuary 2025).

[3] R. M. Botez, P. Molaret, E. Laurendeau, Laminar flow control on a research wing project presentation covering a three year period, In *Proceedings of the Canadian aeronautics and space institute annual general meeting*, 2007.

[4] R. Botez, A. Koreanschi, O. Gabor, Y. Tondji, M. Guezguez, J. Kammegne, L. Grigorie, D. Sandu, Y. Mebarki, M. Mamou, Numerical and experimental transition results evaluation for a morphing wing and aileron system. *The Aeronautical Journal*, **122**, 747-784, 2018.

[5] A. V. Popov, R. M. Botez, M. Labib, Transition point detection from the surface pressure distribution for controller design, *Journal of Aircraft*, **45**, 23-28, 2008.

[6] O. Sugar Gabor, A. Koreanschi, R. M. Botez, A new non-linear vortex lattice method: Applications to wing aerodynamic optimizations, *Chinese Journal of Aeronautics*, **29**, 1178-1195, 2016.

[7] C. Liauzun, D. Le Bihan, J.-M. David, D. Joly, B. Paluch, Study of morphing winglet concepts aimed at improving load control and the aeroelastic behavior of civil transport aircraft, *Aerospace Lab*, 1-15, 2018.

[8] R. Ajaj, M. Friswell, E. Saavedra Flores, O. Little, A. Isikveren, Span morphing: a conceptual design study, In *Proceedings of the 53rd AIAA/ASME/ASCE/AHS/ASC structures, structural dynamics and materials conference 20th AIAA/ASME/AHS adaptive structures conference 14th AIAA*, p. 1510, 2012.

[9] D. Communier, R. M. Botez, T. Wong, Design and validation of a new morphing camber system by testing in the price Païdoussis subsonic wind tunnel, *Aerospace*, **7**, 23, 2020.

[10] M. H. Negahban, R. M. Botez, S. E. Razavi, New Method for the Flow Modeling around chord-wise Morphing Airfoil, In *Proceedings of the AIAA SCITECH 2022 Forum*, p. 2574, 2022.
[11] S. E. Razavi, M. H. Negahban, Numerical Investigation of Flow Behavior Around Chordwise Morphing NACA 0012, *Amirkabir Journal of Mechanical Engineering*, **51**, 1411-1426**, 2020**.
[12] L. Yuzhu, G. Wenjie, Z. Jin, Y. Zhang, Z. Donglai, W. Zhuo, D. Dianbiao, Design and experiment of concentrated flexibility-based variable camber morphing wing, *Chinese Journal of Aeronautics*, **35**, 455-469, 2022.
[13] H. Muhammad Umer, A. Maqsood, R. Riaz, S. Salamat, Stability characteristics of wing span and sweep morphing for small unmanned air vehicle: a mathematical analysis, *Mathematical Problems in Engineering* **2020**, 2020.
[14] M. H. Negahban, M. Bashir, R. M. Botez, Aerodynamic Optimization of a Novel Synthetic Trailing Edge and Chord Elongation Morphing: Application to the UAS-S45 Airfoil, In *Proceedings of the AIAA SCITECH 2023 Forum*, p. 1582, 2023.
[15] M. Bashir, S. Longtin-Martel, R. M. Botez, T. Wong, Optimization and design of a flexible droop-nose leading-edge morphing wing based on a novel black widow optimization algorithm - part I, *Designs*, **6**, 10, 2022.
[16] M. Bashir, S. Longtin-Martel, N. Zonzini, R. M. Botez, A. Ceruti, T. Wong, Optimization and Design of a Flexible Droop Nose Leading Edge Morphing Wing Based on a Novel Black Widow Optimization (BWO) Algorithm - Part II, *Designs*, **6**, 102, 2022.
[17] K. Zi, L. Daochun, S. Tong, J. Xiang, L. Zhang, Aerodynamic characteristics of morphing wing with flexible leading-edge, *Chinese Journal of Aeronautics*, **33**, 2610-2619, 2020.
[18] N. Ismail, A. Zulkifli, M. Abdullah, M. H. Basri, N. S. Abdullah, Optimization of aerodynamic efficiency for twist morphing MAV wing, *Chinese Journal of Aeronautics*, **27**, 475-487, 2014.
[19] S. Powers, L. Webb, E. Friend, W. Lokos, Flight test results from a supercritical mission adaptive wing with smooth variable camber, In *Proceedings of the 6th AIAA Biennial Flight Test Conference*, p. 4101, 1992.
[20] E. Ting, D. Chaparro, N. Nguyen and G. E. Fujiwara, Optimization of variable-camber continuous trailing-edge flap configuration for drag reduction, *Journal of Aircraft*, **55**(6): p. 2217-2239, 2018.
[21] E. Ting, D. Chaparro, and N. T. Nguyen, Aero-structural optimization of variable camber continuous trailing edge flap configurations using transonic and viscous potential flow method, i*n 35th AIAA Applied Aerodynamics Conference*, p. 4220, 2017.
[22] J. Urnes and N. Nguyen, A mission adaptive variable camber flap control system to optimize high lift and cruise lift to drag ratios of future n+ 3 transport aircraft, in *51st AIAA aerospace sciences meeting including the new horizons forum and aerospace exposition*, p. 214, 2013.
[23] B. K. Woods, L. Parsons, A. B. Coles, J. H. Fincham, M. I. Friswell, Morphing elastically lofted transition for active camber control surfaces, *Aerospace Science and Technology*, **55**: p. 439-448, 2016.
[24] D. Ninian and S. M. Dakka, Design, development and testing of shape shifting wing model, *Aerospace*, **4**(4): p. 52, 2017.
[25] Z. Lyu and J. R. Martins, Aerodynamic shape optimization of an adaptive morphing trailing-edge wing, J*ournal of Aircraft*, **52**(6): p. 1951-1970, 2015.
[26] D. Communier, R. Botez and T. Wong, Experimental validation of a new morphing trailing edge system using Price–Païdoussis wind tunnel tests, *Chinese Journal of Aeronautics*, **32**(6): p. 1353-1366, 2019.
[27] M. R. Khorrami, D. P. Lockard, J. B. Moore, J. Su, T. L. Turner, J. C. Lin, K. M. Taminger, S. K. Kahng, S. A. Verden, *Elastically deformable side-edge link for trailing-edge flap aeroacoustic noise reduction*, 2014.
[28] A. E. Rivero, S. Fournier, M. Manolesos, J. E. Cooper, B. K. Woods, Experimental aerodynamic comparison of active camber morphing and trailing-edge flaps, *AIAA Journal*, **59**(7): p. 2627-2640, 2021.
[29] M. Towara and U. Naumann, A discrete adjoint model for OpenFOAM, *Procedia Computer Science*, **18**: p. 429-438, 2013.
[30] P. He, C. A. Mader, J. R. Martins and K. J. Maki, Dafoam: An open-source adjoint framework for multidisciplinary design optimization with openfoam, *AIAA journal*, **58**(3): p. 1304-1319, 2020.
[31] T. Sederberg, Free-form deformation of solid geometric models, *Computer Graphics (SIGGRAPH)*, **26**: p. 151, 1992.
[32] S. Coquillart, Extended free-form deformation: A sculpturing tool for 3D geometric modeling, in *Proceedings of the 17th annual conference on Computer graphics and interactive techniques*, 1990.
[33] H. J. Lamousin and N. Waggenspack, NURBS-based free-form deformations, *IEEE Computer Graphics and Applications*, **14**(6): p. 59-65, 1994.
[34] A. Ronzheimer, Shape parameterisation based on freeform deformation in aerodynamic design optimization, *ERCOFTAC Design Optimization: Methods & Applications*, **400**, 2004.

[35] T. W. Sederberg and S. R. Parry, Free-form deformation of solid geometric models, in *Proceedings of the 13th annual conference on Computer graphics and interactive techniques*, pp. 151-160, 1986.
[36] J. Samareh, Multidisciplinary aerodynamic-structural shape optimization using deformation (MASSOUD), in *8th Symposium on Multidisciplinary Analysis and Optimization*, p. 4911, 2000.
[37] J. F. Marchman, *Aerodynamics and aircraft performance*, 3rd edition, Copyright Year: 2004, ISBN 13: 9781949373639, Publisher: Virginia Tech Libraries 2004.